Infrared Spectroscopy of Prereactive Aluminum−, Gallium−, and Indium−HCN Entrance Channel Complexes Solvated in Helium Nanodroplets[†]

Jeremy M. Merritt,* Gary E. Douberly,[‡] Paul L. Stiles,[§] and Roger E. Miller[#]

Department of Chemistry, University of North Carolina at Chapel Hill, Chapel Hill, North Carolina 27599

Received: June 26, 2007; In Final Form: July 29, 2007

Prereactive metal atom−HCN entrance channel complexes [M−HCN (M = Al, Ga, In)] have been stabilized in helium nanodroplets. Rotationally resolved infrared spectra are reported for the CH stretching vibration of the linear nitrogen-bound HCN−Ga and HCN−In complexes that show significant perturbation due to spin−orbit coupling of the $^2\Pi_{1/2}$ ground state with the $^2\Sigma_{1/2}$ state which are degenerate at long range. Six unresolved bands are also observed and assigned to the linear hydrogen-bound isomers of Al−HCN, Ga−HCN, and In−HCN corresponding to the fundamental CH stretching vibration and a combination band involving the CH stretch plus intermolecular stretch for each isomer. A nitrogen-bound HCN−Al complex is not observed, which is attributed to reaction, even at 0.37 K. This conclusion is supported by the observation of a weakly bound complex containing two HCN's and one Al atom which, from the analysis of its rotationally resolved zero-field and Stark spectra is assigned to a weakly bound complex of a HCNAl reaction product and a second HCN molecule. Theoretical calculations are presented to elucidate the reaction mechanisms and energetics of these metal atom reactions with HCN.

Introduction

The torques experienced by reactive species due to long-range forces, albeit weak, have recently been found to have a considerable influence on reaction dynamics.[1−6] Near threshold reactions and reactions occurring at ultracold temperatures have been found to be particulary sensitive to these effects. Indeed, neglecting the weak van der Waals interactions in the Cl + HD reaction gives a qualitatively wrong picture of the branching ratio at low temperature,[1] emphasizing the need to characterize these regions of the potential energy surface.

Spectroscopic studies of weakly bound complexes have allowed the interrogation of intermolecular potential energy surfaces at an unprecedented level of detail.[7] Though most of these studies have concentrated on complexes containing unreactive, closed-shell, atoms and molecules, some progress has also been made in the stabilization of open-shell, prereactive van der Waals clusters.[8−12] For cluster systems where the associated barriers to reaction are low, it may be possible to initiate the corresponding reaction using electronic or vibrational excitation. Experiments of this type are particularly interesting, given the fact that impact parameter averaging can be largely eliminated, which is the major hurdle in comparing theoretical calculations and results from reactive scattering. In addition, if the system can be given just enough energy to overcome the reaction barrier, the product branching ratios and final state distributions should be most sensitive to the details of the potential energy surface. An important question in induced photochemistry is how the initial bright state couples to the reaction coordinate. For cluster systems the competition between predissociation and reaction is particularly relevant. Recent theoretical time-dependent wavepacket studies on Cl(^{2}P)−HCl[13] show that vibrational excitation of HCl to its first overtone results in nearly equal probabilities of reaction and dissociation.

Stabilizing weakly bound prereactive complexes is challenging experimentally. Although free jet expansions have been succesfully applied to certain systems, the relatively warm conditions early in the expansion are disadvantageous. In recent years helium nanodroplets have emerged as a nearly ideal matrix to study weakly interacting complexes,[14] including open-shell entrance channel complexes.[15] Sequential pickup and independent cooling to the droplet temperature of 0.37 K ensures that the reactants come together with minimal excess energy, thus allowing prereactive complexes to be stabilized behind even small barriers. In this study we apply helium nanodroplets to the stabilization and study of highly reactive metal atom−HCN complexes.

The reactions of aluminum and gallium atoms have also drawn considerable experimental[16−18] and theoretical[19−24] attention in their own right with regard to understanding their elementary reactions that are important to chemisorption and catalysis. These metal atoms are so reactive that aluminum is used in solid rocket propellant, where it can react exothermically with the products of combustion of other fuels, including HCl, H_2O, CO, and CO_2. Currently there is very little known about the elementary reactions or even thermochemistry of many of the involved species.

Previous Argon Matrix Results

The chemical reactions of B, Al, Ga, In, and Tl atoms with HCN have been studied by Andrews et al.[17,25] in a solid argon matrix. In each case the MCN, MNC, and MH postreaction products were identified in the matrix using infrared spectros-

Al−, Ga−, In−HCN Entrance Channel Complexes

J. Phys. Chem. A, Vol. 111, No. 49, 2007 **12305**

copy. Secondary broad-band UV photolysis was found to increase the population of MCN at the expense of MNC for M = Ga, In, and Tl. The authors reasoned this behavior by assuming that MNC was initially favored in the deposition, due to its lower energy, and that UV photolysis equilibrates the two isomers given that the photon has sufficient energy to overcome the barrier to interconversion. Electronic structure calculations (at the DFT-BP86/6-311G(d)-LANL2DZ level) were used to support their findings. In the Al + HCN reaction, MCN and MNC grew upon photolysis, suggesting photolytic decomposition of a intermediate reaction product [MHCN]:

$$M + HCN \rightarrow [MHCN]$$

$$[MHCN] + h\nu \rightarrow MNC/MCN + H$$
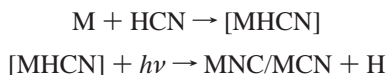
Indeed, from their work on B + HCN,[25] Andrews et al. identified the HBCN, HBNC, and HB(CN) reaction products; however such species were not assigned in the aluminum work. In this work cyclic products will be distinguished by parentheses, and the atom not included in the parentheses is bonded to the hydrogen atom. Despite the prediction of stable complexes that exhibit NH or CH bonds, no experimental evidence for their formation was found, illustrating that the barriers to isomerization to the lower energy products can be surmounted. Given the proven ability of helium droplets to stabilize nonequilibrium structures, the study of reactive systems is of great interest because the associated reaction dynamics could be significantly altered. Ultimately, the reaction might be quenched behind even small barriers allowing the study of exotic species such as HC-(NM) and HN(CM), which would improve our understanding of metal−ligand bonding.

Experimental Section

The experimental apparatus used in the current study has been described in detail previously.[26] Helium droplets are formed by expanding ultrahigh-purity helium gas through a 5 μm pinhole nozzle that is cooled to 23−14 K by a closed-cycle helium refrigerator. The backing pressure of the nozzle was 50 bar, resulting in the formation of droplets with a mean size of 3000−10000 helium atoms.[27] Because the droplet size ultimately limits the available coolant to the reaction, larger droplets will be needed to stabilize more highly exothermic reaction products. The expansion is skimmed by a 0.4 mm diameter skimmer about 1 cm downstream from the nozzle, which is necessary to provide the differential pumping needed to prevent contamination of the droplets by background gas, and to form a beam.

Pick-up cross-sections of the droplets have been determined to be 50−90% of the geometric collision cross-section,[28] requiring low background pressures to prevent contamination. As a result, only very low vapor pressures are needed to intensionally dope the droplets, which is an important consideration for nonvolatile species. Pulsed laser ablation methods are routinely used for seeding metal atoms and their clusters into pulsed free jet expansions, and recently this technique has been demonstrated for helium droplet doping as well.[29] The low duty-cycle that would result from our continuous-wave lasers, however, required a conventional thermal heating source. In this work a resistively heated alumina crucible was used to generate sufficient vapor pressure of the metals for pickup. An oven temperature of approximately 1400 K was needed to dope the droplets with a single aluminum atom, corresponding to a vapor pressure of 10^{-3} to 10^{-4} Torr. Somewhat lower temperatures were required for Ga and In due to their higher vapor pressures. The effusive metal atom source was positioned such that the

droplet beam passed directly over the opening of the crucible, which has an area of 1 cm^2 and is enclosed in a water-cooled copper box with holes to allow the helium droplet beam to enter and exit. HCN molecules are picked up downstream using a differentially pumped scattering chamber maintained at a pressure to optimize for the pickup of just one HCN molecule. To optimize the experimental conditions for a metal atom−HCN complex, the oven temperature was increased until the laser induced signal from HCN monomer was slightly reduced, signifying that some of the droplets have been doped with the metal atoms.

At the temperature of the oven, significant population of the upper spin−orbit component of Al and Ga is expected. In a recent study of Al atoms solvated in helium droplets no evidence for Al($^2P_{3/2}$) was observed,[30] which is consistent with the fast (nanosecond or subnanosecond) relaxation among the spin orbit states of alkali atoms solvated in bulk liquid helium.[31] Given that the flight time between the metal oven and HCN pick-up cell is on the order of 100 μs, we expect that the full population is cooled into the lower $\Omega = {}^1/_2$ levels before complexation. Due to differential pumping and shielding of the oven, reaction of HCN inside the oven is also expected to be negligible.

Vibrational excitation of the embedded chromophore is performed with an F-center laser (Burleigh FCL-20) operating on crystal #3 (RbCl:Li), which is pumped by a krypton ion laser. Details on the tuning behavior and frequency calibration are given elsewhere.[32,33] The droplet beam is aligned such that it impinges upon a liquid helium cooled bolometer that is used to measure the on-axis droplet beam flux. Vibrational excitation and subsequent relaxation of the chromophore results in the evaporation of about 600 helium atoms for a 3000 cm^{-1} photon.[34] By mechanically chopping the laser beam, the corresponding change in the droplet beam flux, due to vibrational excitation, is monitored with a lock-in amplifier. To increase the laser−droplet beam interaction length, a parallel multipass cell was used resulting in approximately 30 orthogonal laser crossings. The multipass cell is also equipped with two parallel electrodes so that Stark and pendular spectroscopy can be performed.[35,36] The laser polarization was oriented parallel with the electric field vector resulting in $\Delta M = 0$ selection rules. Procedures for the calibration of the electric field are described elsewhere.[37]

## Nonrelativistic *ab Initio* Calculations

To survey the potential energy surfaces (PES) of Ga and Al + HCN, we have computed the energies of the stationary points employing the composite CBS-Q[38] and G2[39] methods and also at the UCCSD(T)/6-311++G(d,p) level using Gaussian 03.[40] Table 1 summarizes the results of these calculations, which include a zero-point energy correction based on harmonic frequency calculations performed at the same level. The vibrational frequencies were also used to confirm the nature of the stationary point; potential minima were found to have all real frequencies, and transition states had exactly one imaginary frequency. A graphical representation of the HCN + Ga PES calculated at the G2 level is shown in Figure 1. HC(GaN) and HCNGa could not be stabilized in the G2 calculations, so we scaled the CBS-Q energy to match the G2 results for HGaCN. Optimized geometrical parameters for the reaction products and transition states of the Ga + HCN surface are shown in Figures 2 and 3, respectively, calculated at the UMP2(full)/6-31G(d,p), RMP2/aug-cc-pVDZ, and UCCSD(T)/6-311++G(d,p) levels.

In the Ga + HCN reaction, HGaCN is found by all methods to be the global minimum, being bound by -12.95 kcal mol^{-1}

12306 *J. Phys. Chem. A, Vol. 111, No. 49, 2007*

Merritt et al.

TABLE 1: *Ab Initio* Energies for the Stationary Points on the Ga (Al) + HCN Potential Energy Surface[a]

species	CBS-Q	G2	UCCSD(T)/ 6-311++G(d,p)
HCN + Ga (Al)	0.0 (0.0)	0.0 (0.0)	0.0 (0.0)
GaH (AlH) + CN	57.53 (53.71)	59.12 (54.52)	59.07 (53.77)
H + GaCN (AlCN)	15.42 (10.11)	18.54 (10.57)	20.11 (10.05)
H + GaNC (AlNC)	14.85 (3.50)	29.46 (5.04)	22.86 (5.71)
HCN-Ga (HCN−Al)	−5.58 (−4.39)	−4.10 (−4.23)	−2.88 (−3.95)
Ga-HCN (Al−HCN)	−4.38 (−2.51)	−2.27 (−2.27)	−1.85 (−2.77)
HGaCN (HAlCN)	−15.64 (−30.39)	−12.95 (−29.61)	−8.42[e] (−27.35)
HGaNC (HAlNC)	−11.32 (−33.24)	2.00 (−30.75)	−0.91 (−27.53)
HC(GaN) (HC(AlN))	−13.04 (−20.88)	−[d] (−18.43)	−[d] (−14.96)
HCNGa (HCNAl)	−10.94 (−22.28)	−[d] (−19.54)	2.45[c] (−15.91)
TS1	−6.80 (−11.58)	−1.61 (−9.75)	−[b] (−3.31)
TS2	−[b] (−[b])	21.43 (10.51)	−[d] (−[b])
TS3	−5.16 (−[b])	−2.12 (−4.16)	−[b] (−0.77)

[a] Energies are given in kcal mol⁻¹ and include a zero-point energy correction based on a harmonic frequency calculation. [b] No convergence. [c] T1 diagnostic equals 0.040.[41] [d] Excessive core-valence mixing. [e] One imaginary frequency.
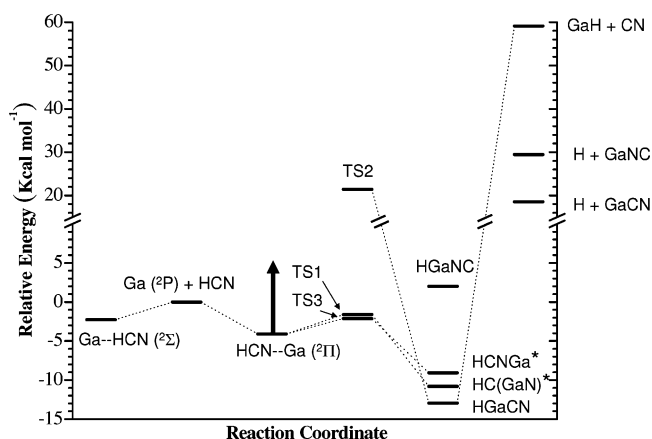
Figure 1. Interaction potential for Ga + HCN calculated at the G2 level. In addition to two weakly bound van der Waals complexes, four reaction products are calculated to be stable. The transition states connecting the entrance channel to the reaction products are also shown for three of the products, and two of these might be surmounted with an infrared photon, tuned to the CH stretch of HCN, as illustrated by the arrow in the figure. G2 calculations for the products labeled with an asterisk did not converge, so the energy in the figure comes from the CBS-Q results, which have been scaled to the G2 results for HGaCN.

at the G2 level. Interestingly, our calculations predict HAlNC is more stable than HAlCN in contrast to gallium. A single transition state connecting HGaCN to the HCN−Ga entrance channel complex (TS2) was found at an energy of 21.43 kcal mol⁻¹ at the G2 level, indicating that HMCN can be formed by the insertion of the metal atom into the CH bond of HCN in a single step. The reaction to form HMNC, however, most likely occurs in two steps, where the metal atom first reacts on the nitrogen end of HCN followed by a migration of the hydrogen atom. Given the rather high energy of H + MNC, it is likely that the barrier to this reaction would be similar to TS2. Two products resulting from metal atom attack on the nitrogen end of HCN are found in our calculations, namely HCNM and HC-(MN), which could be intermediates to HMNC formation. The T1 diagnostic found in the UCCSD(T) calculations for HCNGa is 0.04, suggesting that the ground-state wavefunction has multireference character,[41] and thus the predicted energy should be treated with caution. The gallium and aluminum analogs of HB(CN) could not be converged in our calculations. Table 2 summarizes the harmonic vibrational frequencies of the reaction products calculated at the UCCSD(T)/6-311++G(d,p) and RMP2/aug-cc-pVDZ levels.

In addition to the chemically bound species described above, our calculations predict two linear van der Waals complexes, representing the entrance channel complexes to the associated reactions. Vibrational excitation of the HCN+Ga entrance channel complexes (denoted by the vertical arrow in Figure 1, which is drawn to scale for the CH stretch excitation) might be used to initiate the corresponding reactions. Interestingly, the barrier to form the global minimum product cannot be surmounted with a vibrational photon, suggesting mode selective chemistry could be used to form the less energetically favored products.

## HCN + Ga Two-Dimensional Potential Energy Surfaces

Given the cold conditions characteristic of the droplets, long-range forces are important in governing complexation. To fully understand the long-range interaction potentials for Al, Ga, and In + HCN in their ground states, three adiabatic potential energy surfaces are needed. Due to the fact that the lone unpaired electron of the metal atom resides in a p orbital, upon complexation, the 3-fold degeneracy of the atomic states will be broken, resulting in two states of A′ and one state of A″ in C_s symmetry. For linear geometries, two of these states, one of A′ and one of A″ symmetry, are degenerate, forming the two components of a Π state. The second state of A′ symmetry correlates with a Σ state.

To quantify the potentials for HCN + Ga, we have calculated two-dimensional PES's for the three spin-free adiabatic potentials (1A″, 1A′, 2A′) at the RCCSD(T)/aug-cc-pVDZ+{332} level using MOLPRO,[42] which are shown in Figure 4. The calculations employed Jacobi coordinates, where the vector **R** points from the nuclear center of mass of HCN to gallium, characterized by length R, and θ is the angle between **R** and the HCN symmetry axis. $\theta = 0°$ corresponds to the nitrogen-bound HCN−Ga geometry. Interaction energies were calculated on a grid in which R and θ were incremented in steps of 0.1 Å and 10°, respectively, and a spline interpolation was used to smooth the surface. HCN was constrained to be linear, with bond lengths $r_{CN} = 1.1532$ Å and $r_{CH} = 1.0655$ Å, which were also held fixed. A set of uncontracted midbond functions, with sp exponents 0.9, 0.3, and 0.1 and d exponents 0.6 and 0.2 (denoted as {332}), are added to the aug-cc-pVDZ basis set at the midpoint between the metal atom and the HCN nuclear center of mass. The 1S electrons on carbon and nitrogen, along with the 1S, 2S, 2P, 3S, and 3P electrons on gallium were left uncorrelated in the CCSD(T) calculations. Counterpoise correction was performed using the method of Boys and Bernardi[43] where the lowest RCCSD(T) energy of the free gallium atom was subtracted from both A′ dimer energies preserving the double degeneracy of the Π state for both linear geometries.

For linear HCN−Ga ($\theta = 0°$) the 1A″ and 1A′ states correlate with a doubly degenerate ²Π ground state and the 2A′ state corresponds to an excited repulsive ²Σ state, whereas for linear Ga−HCN ($\theta = 180°$), the 1A″ and 2A′ states correlate with an excited repulsive ²Π state and 1A′ is the ²Σ ground state. This state correlation is opposite to that observed for HCN−Br[44,45] due to the p¹ vs p⁵ electronic configurations of the metal atoms compared to halogen atoms. The ground electronic symmetries are dictated mostly by the electrostatic dipole−quadrupole interaction. Two linear isomers are predicted from the 2D surfaces, with calculated binding energies (D_e) of 1380 and 970 cm⁻¹ for HCN−Ga and Ga−HCN, respectively, in qualitative agreement with the CBS-Q, G2, and UCCSD(T)/6-311++G-(d,p) results given in Table 1. The transition state for isomerization between the two isomers is found at $\theta = 109°$, $R =$
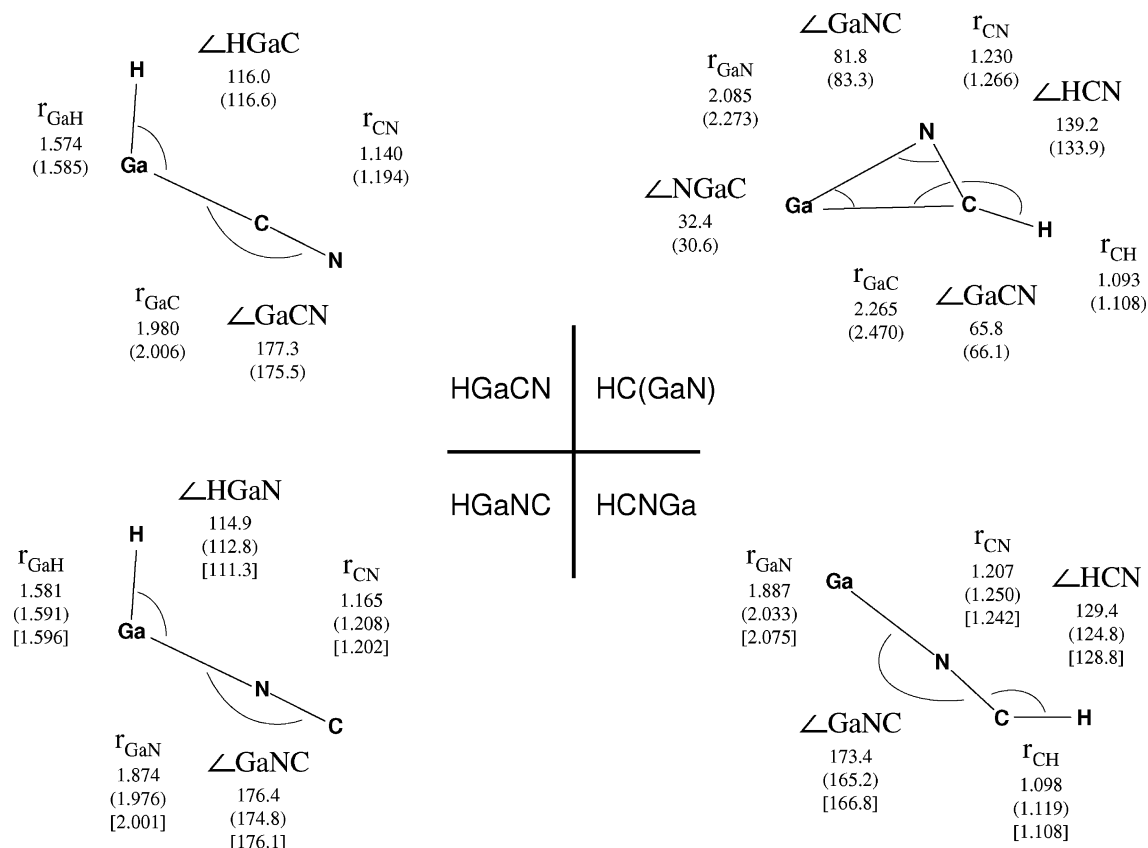
Figure 2. Optimized geometrical parameters for the four reaction products of Ga + HCN, calculated at the UMP2(full)/6-31G(d), (RMP2/aug-cc-pVDZ), and [UCCSD(T)/6-311++G(d,p)] levels.
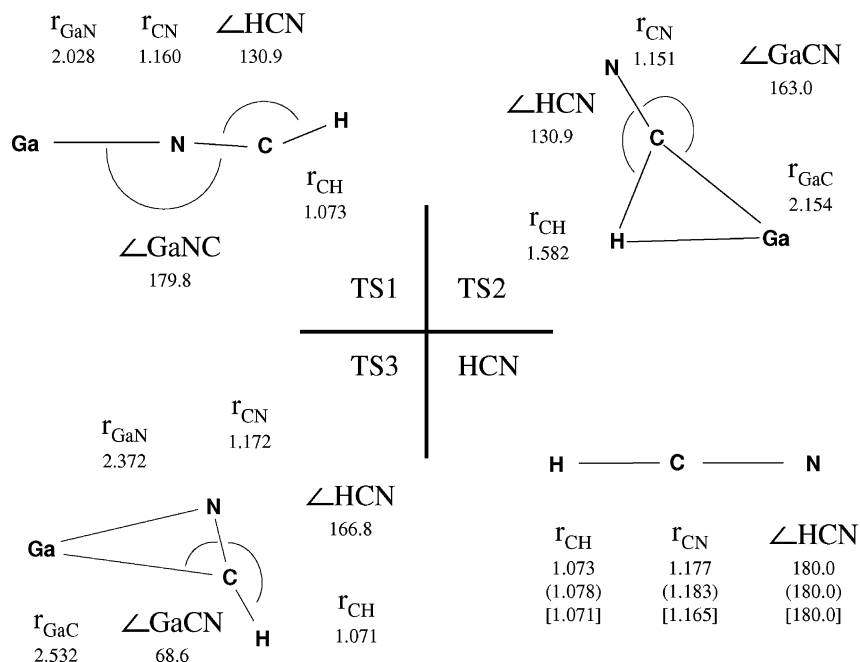
Figure 3. Optimized geometrical parameters for the three transition states connecting the entrance channel complexes to the reaction products for Ga + HCN, and HCN itself, calculated at the UMP2(full)/6-31G(d), (RMP2/aug-cc-pVDZ), and [UCCSD(T)/6-311++G(d,p)] levels.

4.01 Å at an energy of −610 cm^{-1}. Fully relaxed geometry optimizations at the RCCSD(T)/aug-cc-pVTZ level were performed for the M−HCN and HCN−M (M = Al, Ga, In) complexes, and the resulting molecular parameters are given in Table 3. A detailed comparison of these calculations with our experimental results will be presented in the next section. In addition to the two linear minima on the 1A′ surface, a third minimum is observed corresponding to a T-shaped isomer,

similar to that found in the PES's of X−HX (X = F, Cl, Br) complexes.[48,49] This T-shaped minimum may be an important precursor to the formation of the HC(GaN) reaction product at ultracold temperatures due to the similarity in geometry. The carbon−gallium distance of the T-shaped complex is found to be ∼3.0 Å, compared to ∼2.0 Å in the HC(GaN) product. We have not been able to stabilize this weakly bound T-shaped isomer in subsequent geometry optimizations however.

TABLE 2: Harmonic Vibrational Frequencies (in cm^{-1}) for the Gallium and Aluminum Reaction Products with HCN at the UCCSD(T)/6-311++G(d,p) and RMP2/aug-cc-pVDZ Levels, Labeled CC and MP2 Respectively[a]

| | HGaCN | | HAlCN | | HGaNC | | HAlNC | HCNGa | | HCNAl | | HC(GaN) | HC(AlN) | |
	CC	MP2	CC	MP2	CC	MP2	CC	CC	MP2	CC	MP2	MP2	CC	MP2
ν_1	2049 (17)	2381	2047 (20)	2079	2037 (247)		2069	2917	2876 (177)	2900	2911 (215)	3029 (24)	3035	3054 (12)
ν_2	1924 (208)	1929	1927 (198)	1813	1903 (160)		1907	1943	1804 (344)	1840	2052 (81)	2049 (40)	1753	1692 (9)
ν_3	580 (97)	607	604 (190)	572	586 (76)		620	969	916 (131)	988	959 (228)	1131 (84)	978	1130 (47)
ν_4	430 (82)	525	510 (74)	519	464 (106)		584	459	474 (206)	562	532 (180)	596 (57)	620	631 (36)
ν_5	205 (5)	207	206 (6)	152	141 (2)		162	141	133 (0)	166	181 (11)	399 (102)	470	456 (150)
ν_6	194 (4)	191	195 (4)	141	117 (2)		148	115	113 (0)	156	157 (10)	204 (43)	264	307 (49)

[a] Values in parentheses are the calculated transition intensities in km mol^{-1}.

TABLE 3: Summary of Molecular Properties for the HCN−M and M−HCN Complexes (M = Al, Ga, In) Calculated at the RCCSD(T)/aug-cc-pVTZ Level[a]

RCCSD(T) aug-cc-pVTZ	HCN−Al (Al−HCN)	HCN−Ga (Ga−HCN)	HCN−Ga (ECP) (Ga−HCN (ECP))	HCN−In (ECP) (In−HCN (ECP))
R (Å)	2.565 (4.938)	3.302 (4.882)	3.330 (4.904)	3.567 (5.092)
r_{CH} (Å)	1.067 (1.073)	1.067 (1.073)	1.068 (1.073)	1.068 (1.073)
r_{CN} (Å)	1.182 (1.161)	1.152 (1.154)	1.152 (1.154)	1.152 (1.154)
B_e (cm^{-1})	0.167 (0.049)	0.075 (0.035)	0.074 (0.035)	0.058 (0.029)
ν_{shift} (cm^{-1})	b (−93.83)	−2.47 (−95.39)	−2.42 (−91.30)	−2.09 (−88.80)
μ (D)^c	− (3.79)	4.50 (3.77)	4.39 (3.81)	4.40 (3.87)
ν_{vdws} (cm^{-1})	− (69.14)	75.74 (54.58)	78.33 (52.87)	76.79 (46.51)

[a] The calculations labeled "(ECP)" employed a small core relativistic pseudopotential (aug-cc-pVTZ-PP[47]) on the metal atom. ν_{vdw} is the energy of the intermolecular stretching mode, obtained from harmonic frequency calculations. ν_{shift} is the predicted frequency shift of the CH stretching vibration of HCN upon complexation, calculated by subtracting the frequency calculations for the metal−HCN complex from a separate fully optimized calculation on the HCN monomer. ^{b} One imaginary frequency. ^{c} Finite field approximation.[46]
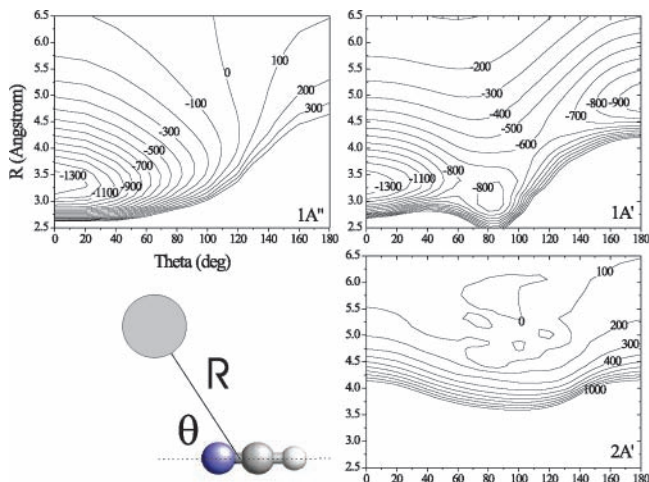
Figure 4. 2D potential energy surfaces for the 1A″, 1A′, and 2A′ symmetries of HCN+Ga calculated at the RCCSD(T)/aug-cc-pVDZ+{332} level. Basis set superposition error has been removed using counterpoise correction.

1-D Relativistic Adiabatic Calculations

Spin−orbit coupling (SOC) can reshape potential energy surfaces,[49,50] and to make detailed comparisons with our experiment, we must incorporate it into our calculations. For the linear geometries (1D slices) of our 2D *ab initio* potentials we take note of the operator form of the spin−orbit Hamiltonian:

$$H^{so} = A(\mathbf{L} \cdot \mathbf{S})$$

$$= A\left(L_z S_z + \frac{L^+ S^- + L^- S^+}{2} \right)$$

The spin−orbit coupling constant, A, is 74.7, 551, and 1475 cm^{-1} for Al, Ga, and In, respectively.[51] Note that A is positive illustrating that the $^2P_{1/2}$ state lies below the $^2P_{3/2}$ state in the free atoms, where the reverse is true for halogen atoms.

One-dimensional relativistic adiabatic potential energy surfaces for HCN + M are found by diagonalizing the (R-dependent) matrix:

$$\begin{bmatrix} ^2\Sigma & (2^{-1/2}A) & 0 \\ (2^{-1/2}A) & ^2\Pi - A/2 & 0 \\ 0 & 0 & ^2\Pi + A/2 \end{bmatrix}$$

assuming that SOC is independent of geometry. The eigenvalues of this matrix are the energies of the $^2\Sigma_{1/2}$, $^2\Pi_{1/2}$, and $^2\Pi_{3/2}$ states. Diagonalized 1-D relativistic and nonrelativistic adiabatic potentials for HCN + Ga calculated at the RCCSD(T)/aug-cc-pVTZ+{332} are shown in Figure 5. The legend for the $^2\Sigma_{1/2}$ and $^2\Pi_{1/2}$ states corresponds to the basis function with the largest mixing coefficient. Interestingly, the electronic character for the mixed states of the hydrogen-bound isomer invert as the distance is decreased. The lowest energy potential at long range is mostly $^2\Pi - A/2$ like, but in the region of the minimum, it is $^2\Sigma$ like. In the $R \to \infty$ limit, the $^2\Sigma_{1/2}$ and $^2\Pi_{3/2}$ states converge and their separation from the $^2\Pi_{1/2}$ becomes $(3/2)A$, as in the free atom. Bound states supported by the potentials were calculated numerically using the program Level[52] and the binding energies, rotational constants, and van der Waals stretching frequencies are summarized in Tables 4 and 5. The van der waals (intermolecular) stretching frequency is defined as the energy difference between the ground and first excited bound states of our 1D potentials. To estimate the effects of vibrational excitation of the CH stretch of HCN on the potentials, computations were also performed with $r_{CH} = 1.09$ Å, which is close to the vibrationally averaged bond length for the $v = 1$ state. In general, the excitation of HCN results in a slight increase in the binding energy of the complex which we attribute to an increased dipole−quadrupole interaction due to the increased dipole moment of HCN in the excited state.

As noted above, SOC can strongly influence the potentials, and indeed the dissociation energies of the gallium and indium complexes are significantly lowered due to the large SOC and the asymptotic degeneracy of the $^2\Sigma$ and $^2\Pi$ states. The positions of the minima, which are reflected by the B values, are not as strongly affected due to the large energy separation of the $^2\Sigma$ and $^2\Pi$ states in the region of the minimum. Also, the spin−

Al−, Ga−, In−HCN Entrance Channel Complexes

J. Phys. Chem. A, Vol. 111, No. 49, 2007 **12309**

TABLE 4: Summary of the Molecular Parameters Derived from the Bound States of One-Dimensional Potential Energy Surfaces for HCN−Ga and HCN−In[a]

| constant (cm^{-1}) | HCN−^{69}Ga | | HCN−In[b] | |
$v = 0$ ($v = 1$)	$^2\Pi$	$^2\Pi_{1/2}$	$^2\Pi$	$^2\Pi_{1/2}$
D_0	1403.84 (1409.11)	1147.46 (1152.60)	1378.87 (1383.68)	800.98 (805.71)
B_0	0.0813 (0.0813)	0.0808 (0.0808)	0.0629 (0.0629)	0.0608 (0.0609)
ν_{vdws}	76.71 (76.95)	75.08 (75.27)	77.28 (77.52)	66.61 (67.00)
A		551		1475

[a] A is the atomic spin−orbit coupling constant used in the calculations and ν_{vdws} is the van der Waals stretching frequency, defined as the energy separation between the two lowest calculated bound states. For the "$v = 1$" calculations, r_{CH} was fixed at 1.09 Å (compared to 1.0655 Å for $v = 0$) to estimate the effects of vibrational excitation of the HCN. No bound states were found on the $^2\Sigma_{1/2}$ surfaces of the nitrogen-bound geometries. Bound states of the HCN−M complexes correlating with $^2\Pi_{3/2}$ are the same as those given for $^2\Pi$. Due to convergence problems, potential surfaces for HCN−Al could not be constructed. [b] This calculation was performed with the aug-cc-pVTZPP+{332} basis set.[47]

TABLE 5: Summary of the Molecular Parameters Derived from the Bound States of One-Dimensional Potential Energy Surfaces for the Hydrogen-Bound M−HCN Complexes[a]

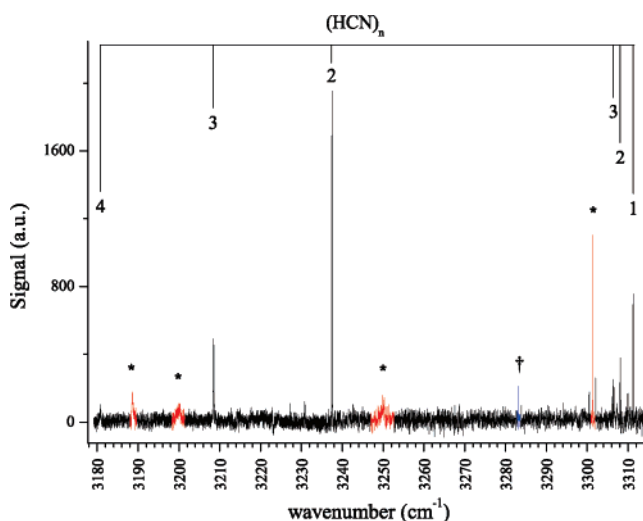| constant (cm^{-1}) | Al−HCN | | ^{69}Ga−HCN | | | In−HCN[b] | | |
$v = 0$ ($v = 1$)	$^2\Sigma$	$^2\Sigma_{1/2}$	$^2\Sigma$	$^2\Sigma_{1/2}$	$^2\Pi_{1/2}$	$^2\Sigma$	$^2\Sigma_{1/2}$	$^2\Pi_{1/2}$
D_0	767.72 (811.73)	695.83 (739.69)	790.61	401.27 (439.16)	97.97	800.52	223.12 (244.25)	330.79
B_0	0.04973 (0.05023)	0.04972 (0.05022)	0.03549	0.03496 (0.03540)	0.02822	0.02927	0.02781 (0.02815)	0.02698
ν_{vdws}	59.30 (61.21)	59.19 (61.11)	46.81	43.13 (44.22)	17.40	45.57	30.52 (31.72)	27.00

[a] ν_{vdws} is the van der Waals stretching frequency, defined as the energy separation between the two lowest calculated bound states. For the "$v = 1$" calculations, r_{CH} was fixed at 1.09 Å (compared to 1.0655 Å for $v = 0$) to estimate the effects of vibrational excitation of the HCN. No bound states were located on the Al−HCN $^2\Pi_{1/2}$ surface. [b] This calculation was performed with the aug-cc-pVTZPP+{332} basis set.[47]
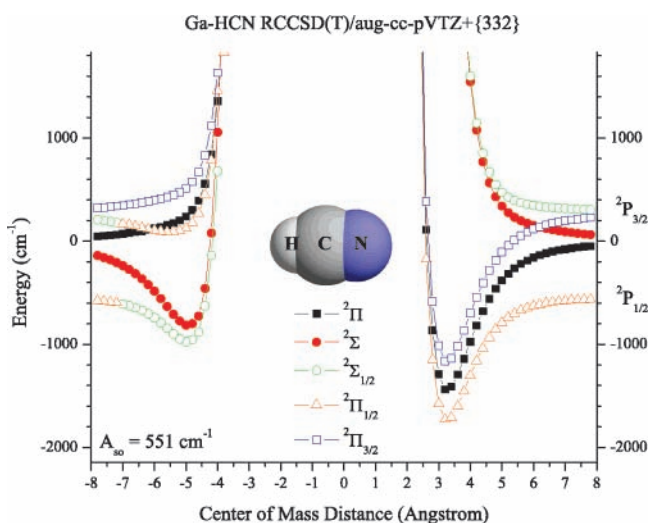
Figure 5. Relativistic and nonrelativistic adiabatic potential energy curves for the HCN−Ga complex calculated at the RCCSD(T)/aug-cc-pVTZ+{332} level.


Figure 6. Pendular survey scan indicating the presence of gallium related complexes (marked with an asterisk). The peak marked with a † optimized for the pickup of a gallium atom, however, also increased when air was introduced into the pick-up cell and so it is related to an impurity. We assign the peak at 3301 cm^{-1} to the nitrogen-bound HCN−Ga complex. Numbered tic marks above the scan correspond to the previously assigned linear chains of HCN.

orbit interaction for the Ga−HCN and In−HCN complexes is sufficiently large that a minimum develops in the upper $^2\Pi_{1/2}$ state. Because the $^2\Pi_{1/2}$ states of the M−HCN complexes, and the $^2\Pi_{3/2}$ states of the HCN−M complexes, correlate with the excited spin−orbit component of the atom, we would not expect these states to be populated in helium droplets.

Experimental Results

Our experimental investigation for Ga + HCN starts with the pendular survey scan shown in Figure 6. The large dc electric field quenches free rotation of the complexes, resulting in a single intense peak near the band origin. This scan was recorded with the gallium oven heated to approximately 1200 K and the helium droplet source conditions optimized for a mean droplet size of 10000 atoms. The numbered tick marks above the scan show the absorptions of the linear chains of HCN,[53] including both free and bonded fundamentals of the CH stretching vibrations. The peaks that grow in as the gallium oven

temperature is increased are highlighted in the figure with an * or †. According to the harmonic vibrational frequency calculations in Tables 2 and 3, only the weakly bound van der Waals complexes should absorb in this spectral region, so the observation of five new peaks hints that higher order clusters are being formed. To sort out the contributions due to higher order HCN clusters, pick-up cell (PUC) pressure dependence measurements were performed. These results are shown in Figure 7 and were obtained by individually recording the signal intensity as a function of the HCN PUC pressure while the laser is tuned to the peak of each absorption. The peaks at 3301.30 and 3249.88 cm^{-1} are found to optimize at the same pressure as HCN monomer confirming they are related to just one HCN. The peak at 3199.77 cm^{-1} optimizes at very high HCN pressure,
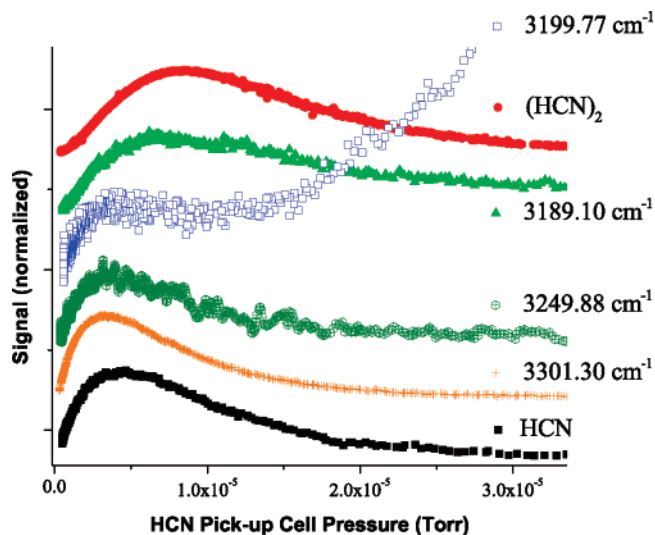
Figure 7. HCN pick-up cell pressure dependencies of the peaks attributed to gallium related complexes in the pendular survey scan of Figure 6. The intensities of three of the peaks are observed to optimize at the same pressure as HCN monomer, suggesting they are all related to 1:1 complexes.

going off-scale in Figure 7; however a shoulder is observed that peaks near the optimum pressure for a single HCN. Such behavior is a consequence of a higher order HCN complex overlapping a complex containing just one HCN at this frequency. The band at 3189.10 cm^{-1} optimizes at nearly double the pressure of HCN monomer, in good agreement with the PUC curve for HCN dimer, suggesting this peak results from a complex of gallium with two HCN's. The peak at 3283 cm^{-1}, marked by an † in the pendular scan, is not included in Figure 7; however, it was also found to optimize at the same pressure as HCN monomer. The intensity of this peak increased when air was introduced into the pick-up cell and thus we preliminarily assign it to an N_2-HCN−Ga complex. All peaks were found to optimize at the same gallium oven temperature.

HCN−Ga. We assign the most intense peak in the survey scan at 3301.29 cm^{-1} to the nitrogen-bound HCN−Ga complex based on the observed frequency shift of −9.91 cm^{-1} from the HCN monomer. Although this frequency shift is somewhat larger than the *ab initio* value of −2.47 cm^{-1} predicted by the harmonic frequencies (see Table 3), it is clearly not in the region predicted for the Ga−HCN complex. From our 1D PES's which include SOC we find that the binding energy of the complex is increased by 5.14 cm^{-1} upon vibrational excitation of the HCN (see Table 4). Neglecting dynamical coupling of the different dimensions of the PES, this change in the binding energy upon excitation would result in a red shift in the vibrational frequency of the same value, improving the agreement with experiment. Interestingly a similar comparison based on the non-spin−orbit corrected potentials yields a red shift of −5.27 cm^{-1}, illustrating that spin−orbit coupling does not significantly effect the vibrational frequency shift of this complex.

Turning off the electric field we recover the spectrum shown in Figure 8A, which clearly exhibits rotational fine structure. To extract the inertial parameters, the spectrum is accompanied by two simulations using different $^2\Pi_{1/2}$ model Hamiltonians. The rotational temperature encorporated in both models has been fixed at 0.37 K, in accord with the droplet temperature.[34,54] In the first simulation (B), we assume a "standard" $^2\Pi_{1/2}$ model, and that the fine structure is due to individual rotational transitions. Descrepancies are observed in the Q-branch intensity
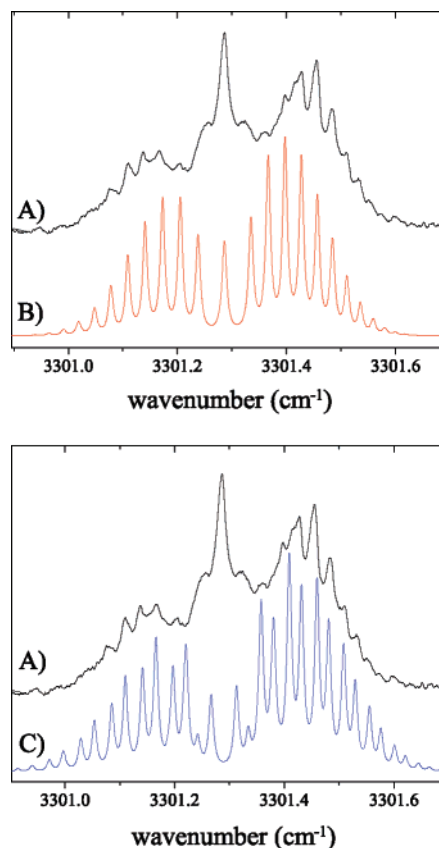
Figure 8. Zero-field spectrum (A) of the band at 3301 cm^{-1}, which we assign to the HCN−Ga complex. In the upper panel (B) the spectrum is simulated using a $^2\Pi_{1/2}$ model that effectively neglects the off-diagonal SOC, whereas on the bottom (C), the spin−orbit coupling has been incorporated to first order. The later simulation shows large parity splittings that may resolve the discrepancy in the rotational constant reduction factor observed.

TABLE 6: Summary of the Fitted Molecular Constants for the HCN−Ga Complex Using Two Different Model Hamiltonians[a]

HCN−Ga	standard $^2\Pi_{1/2}$	perturbed $^2\Pi_{1/2}$
ν_{shift} (cm^{-1})	−9.86	−9.86
B (cm^{-1})	0.0163	0.0270
D (cm^{-1})	7×10^{-6}	5×10^{-6}
Δ (cm^{-1})	>10000	2000

[a] In our "standard" model of a $^2\Pi_{1/2}$ complex off-diagonal spin−orbit coupling has been neglected, whereas in the "perturbed" model off-diagonal spin−orbit coupling is turned on. The large discrepancy in the rotational constants is due to a large parity splitting in the perturbed model.

and the peak in the P and R branch intensities. The rotational constant, B, and centrifugal distortion constant, D, used for this simulation are given in Table 6. The rotational constant, B = 0.016(1) cm^{-1}, is a factor of 5.0 smaller than the *ab initio* value of $B_0 = 0.08057$ cm^{-1} derived from the lowest bound state on our 1D RCCSD(T)/aug-cc-pVTZ+{332} potential. Although solvation in helium droplets typically results in a reduction of the rotational constant due to adiabatic following of some of the helium density, this reduction would be somewhat larger than that observed for most systems. A typical value for the reduction factor on a system of this size is 2.5−3.5, although a reduction factor of 5 is not unprecedented.[55,56]

What remains to be discussed is the effect of the off-diagonal SOC on the infrared spectrum. A full description of our approximate model to simulate the spectra is given elsewhere.[57]

Al−, Ga−, In−HCN Entrance Channel Complexes

J. Phys. Chem. A, Vol. 111, No. 49, 2007 **12311**

Briefly, an effective Hamiltonian matrix is setup using parity adapted Hund's case (a) basis functions. As noted above, the important off-diagonal spin orbit matrix element is given as

$$\left\langle {}^2\Pi_{1/2}^{e/f} \left| \frac{A}{2} L^+ S^- \right| {}^2\Sigma_{1/2}^{e/f} \right\rangle = 2^{1/2} \left(\frac{A}{2} \right)$$

The Hamiltonian is then diagonalized to obtain the eigenvalues and eigenvectors and electric-dipole allowed transitions were computed with standard spherical tensor algebra. The results for the HCN−Ga complex are shown in Figure 8C. Qualitatively, the interaction of the ${}^2\Sigma_{\pm 1/2}$ state removes the degeneracy associated with the two ${}^2\Pi_{\pm 1/2}$ states, resulting in parity, or lambda, doubling. The magnitude of the parity splitting incorporated into the simulation derives from the size of the atomic spin−orbit coupling constant, A, and on the energy separation of the ${}^2\Sigma_{1/2}$ and ${}^2\Pi_{1/2}$ states (Δ), which can be estimated from the potential curves of Figure 5. For the simulation shown in Figure 8C, $B = 0.0270$ cm^{-1}, $\Delta = 2000$ cm^{-1}, and $A = 551$ cm^{-1}. If one compares this rotational constant with the *ab initio* value obtained from the 1D surfaces which include SOC, we find that it is a factor of 2.98 smaller, which is in much better agreement with that observed for the majority of molecules in helium droplets. The unsatisfying feature of the new simulation is that the Q-branch transitions are also split, and no longer stack up at the band origin, where substantial intensity is observed experimentally. Using our approximate model, we have also explored the possibility that the vibrational band may take on some ${}^2\Sigma_{1/2} \leftrightarrow {}^2\Pi_{1/2}$ character, due to SOC; however, we estimate that these effects are negligibly small. At present, we attribute the poor agreement of the Q branch to a perturbation induced by the helium solvent, an effect which has been observed previously for a few closed shell linear molecules.[58−60]

Our approximate model used to simulate the spectra of HCN−Ga gives us a physical basis to understand such a large parity splitting in light of off-diagonal SOC; however, the parameter Δ used to fit the spectra is not easily compared with what would be obtained by higher level theoretical treatments. With the aid of the rotational state assignments derived from our simulation, we refit the HCN−Ga spectrum using the energy level expression: $F(J) = BJ(J + 1) - D[J(J + 1)]^2 \pm (p/2)(J + 1/2)$, which is appropriate for a ${}^2\Pi_{1/2}$ state of a linear molecule that exhibits parity splitting. J represents the total angular momentum of the complex, which is a half-integer starting at $J = {}^1/_2$ for the ${}^2\Pi_{1/2}$ ground state, B and D are the rotational and centrifugal distortion constants, respectively, and p is a parity doubling constant. The top (bottom) signs refer to levels of e (f) parity. The band origin, B, and D constants are the same as those given in Table 6 under "perturbed"; however, we extract $p = 0.0286$ cm^{-1} or $p \sim B$. It would be very interesting to perform bound-state calculations encorporating the three intermolecular potentials to extract the expected gas-phase parity splitting. Such a comparison is especially needed in light of the recent observations that the parity splitting in NO is increased,[61] whereas in HCN−Br[44] it appears to be decreased upon solvation in helium droplets.

Ga−HCN. When experimental conditions are optimized for gallium atom pickup, a second new peak is observed at 3200.0 cm^{-1}. The experimental frequency shift from HCN monomer in helium is −111.4 cm^{-1}, in reasonable agreement with our *ab initio* result of −95.94 cm^{-1} for Ga−HCN at the RCCSD-(T)/aug-cc-pVTZ level. Vibrational frequencies of helium solvated rotors are typically shifted less than 0.1% from their gas-phase values, thus allowing a direct comparison with theory.

Complexes having linear hydrogen bonds however, exhibit systematic increases in the frequency shift of the hydrogen-bonded vibrational mode, which has been attributed to decreased vibrational averaging and the induced polarization of the solvent.[14] Using the empirical correction factor suggested by Merritt et al.,[45] we predict that the helium increases the observed red shift for Ga−HCN by 5.97 cm^{-1}, further improving the agreement with theory. Fine structure is not observed for this band so a rotational level analysis in not possible; however, as mentioned above, we have determined that this peak optimizes at the same HCN pressure and Ga oven temperature as the peak we assign to HCN−Ga, which is suggestive of another 1:1 complex.

Close examination of several pendular survey scans revealed a second broad feature at 3249.87 cm^{-1}. HCN pressure and Ga oven temperature dependence measurements clearly show that this band optimizes at the same conditions as the previously assigned Ga+HCN binary complexes. The frequency shift of this band from HCN monomer is −61.3 cm^{-1}, considerably different from both the predicted free and bonded stretches of the two linear complexes. It is tempting to assign this peak to the T-shaped complex which our potential showed a local minimum; however, more telling is the frequency shift of this band from the peak we assign to the hydrogen-bound complex. The energy separation between these two peaks is 49.80 cm^{-1} in good agreement with the calculated harmonic frequency of the van der Waals stretching mode of 54.58 cm^{-1} for the Ga−HCN isomer. We thus assign this peak to a combination band of the Ga−HCN isomer exciting the CH and the intermolecular stretches. Definitive evidence that this peak must correspond to a binary Ga+HCN complex, other than HCN−Ga, was found using infrared−infrared double resonance population transfer experiments, described elsewhere.[62] The calculated harmonic frequency for the intermolecular bending mode is 76.7 cm^{-1}, in much poorer agreement with experiment. Combining these results with those obtained for the Al−HCN and In−HCN complexes, allows us to rule out the bending mode however; see below. Exciting the combination band probes the van der Waals stretching mode in the CH excited state of HCN; however, the harmonic frequency calculations were on the ground state and also neglect SOC. Using 1D bound states that include SOC, we predict the intermolecular stretching frequency to be 44.22 cm^{-1} on the "excited" HCN surface; see Table 5.

Comparisons with Aluminum and Indium

To aid in our interpretation of the gallium results, experiments were performed with aluminum and indium atoms, attempting to observe their respective entrance channel complexes with HCN. The pendular survey scans in Figure 9 show Al, Ga, and In + HCN related peaks, and the 1:1 complexes have been marked with an asterisk (also in color online). Peaks marked with a † correspond to M−(HCN)$_{n>1}$ clusters, determined from HCN pick-up cell pressure measurements.

Al−HCN. First let us focus on the hydrogen-bonded region where we assigned the Ga−HCN complex at 3200.0 cm^{-1}. When the droplets are doped with aluminum atoms and HCN, a strong peak is observed at 3192.07 cm^{-1}, which we assign to Al−HCN, corresponding to a red shift from HCN monomer of 119.13 cm^{-1}. The *ab initio* RCCSD(T)/aug-cc-pVTZ shift for the Al−HCN complex is 93.83 cm^{-1}. *A priori*, one might think that aluminum, with its relatively small SOC ($A = 74.7$ cm^{-1}) should be the most accurately described by the *ab initio* calculations; however, we find the agreement is quite poor. Correcting for the effects of helium solvation on the vibrational
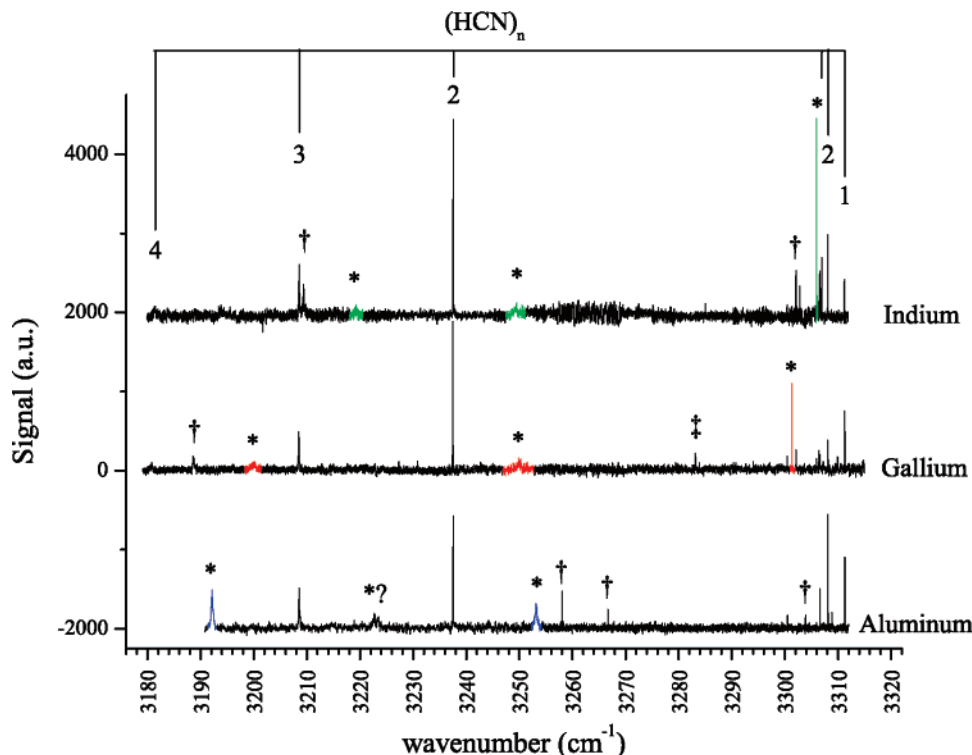
Figure 9. Three pendular survey scans corresponding to separate indium, gallium, and aluminum + HCN experiments. New peaks related to the metal atoms are highlighted and those marked with an asterisk correspond to 1:1 complexes. Peaks marked with a † are related to higher order HCN clusters and the peak marked with a ‡ corresponds to the N_2−HCN−Ga complex.

band origin,[45] we estimate a gas-phase origin of 3198.32 cm^{-1}, or a red shift of 112.88 cm^{-1}, slightly improving the agreement. A second strong peak is observed at 3253.03 cm^{-1}, which we assign to a combination band of the CH and intermolecular stretches, in analogy with the Ga results. From the energy separation between this band and the fundamental, the van der Waals stretching frequency is determined to be 60.96 cm^{-1}. The calculated harmonic frequency for this vibrational mode is 69.14 cm^{-1}, in qualitative agreement with that observed. The intermolecular stretching frequency from our 1D RCCSD(T)/aug-cc-pVTZ+{332} potentials, which incorporate the effects of SOC is 61.11 cm^{-1}, substantially improving the agreement with experiment, thereby lending further support to our assignment. The calculated harmonic frequency for the intermolecular bending mode is 192 cm^{-1}, placing this combination band out of this frequency region.

In−HCN. A third set of experiments have been carried out with indium. Extensive searching led to the identification of the peaks marked with an asterisk in Figure 9, identified as 1:1 complexes, two of which are barely visible at this scale. By comparing with our earlier assignments, the peak at 3219.1 cm^{-1} is assigned to the fundamental CH stretching vibration of In−HCN, and the peak at 3249.11 cm^{-1} to the combination band. The intermolecular stretching frequency is determined to be 30.01 cm^{-1}, in excellent agreement with that determined from our bound-state calculations, namely 31.72 cm^{-1}.

HCN−In. Next let us focus on the free CH stretching region around 3300 cm^{-1}, where we expect the nitrogen-bound complexes to absorb. In agreement with the gallium experiment, a strong peak is observed in the indium survey scan, which we assign to a HCN−In complex. The band origin of this complex is 3306.01 cm^{-1}, red-shifted from HCN monomer by 5.19 cm^{-1}. The calculated frequency shift from the bound states on the 1D potentials is −4.73 cm^{-1}, in substantially better agreement with
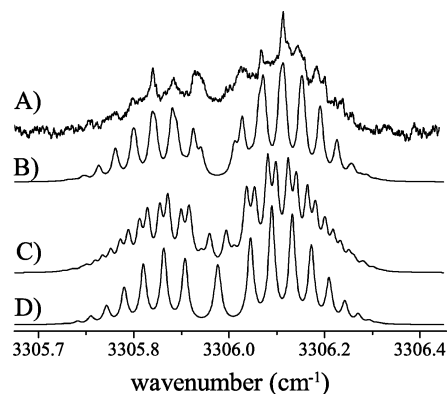
Figure 10. Rotationally resolved zero-field (A) spectrum for the HCN−In complex observed in helium droplets. A series of simulations (B)−(D) are also shown, which illustrate the effect of the transition from Hund's case (a) to case (c) on the possible spectra. Δ = 2000, 6415, and 10000 cm^{-1} for simulations B, C, and D, respectively.

experiment than the harmonic frequency shift of −2.09 cm^{-1}. The field-free spectrum for this band is shown in Figure 1A.

In agreement with the HCN−Ga spectrum, we find that the field-free spectrum of HCN−In does not fit well to a "standard" $^2\Pi_{1/2}$ model Hamiltonian, shown as Figure 10D, which is the result of strong off-diagonal SOC. Instead, the spectrum more appropriately conforms to Hund's case (c) rather than case (a). A simulation using intermediate coupling is shown in Figure 10B, corresponding to Δ = 2000 cm^{-1}, the same Σ−Π separation as that used in the simulation of the HCN−Ga spectrum. That the parity splitting is much larger is due to the larger SOC constant for indium. The fact that both HCN−Ga and HCN−In require similar Δ parameters is reasonable based on their 1D potential energy surfaces. The rotational constant obtained from the simulation of the experimental spectrum is
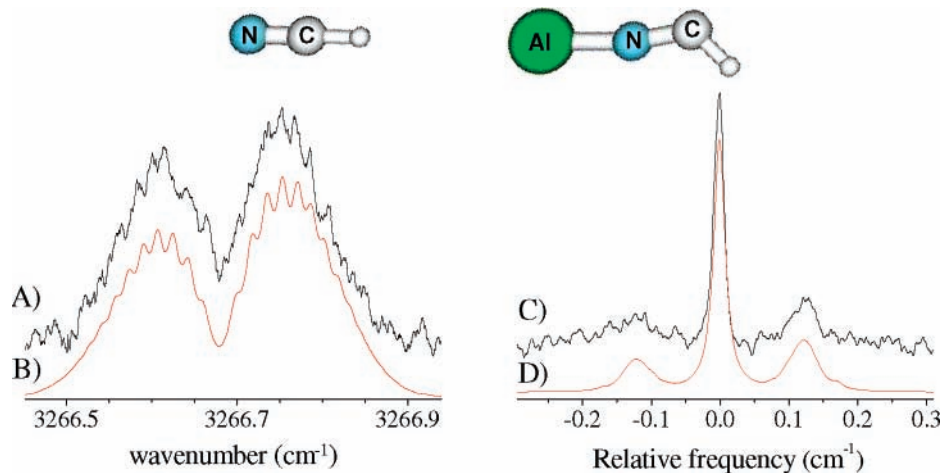
Figure 11. Field-free (A) and Stark spectra (C) for a band that we preliminarily assign to a complex between a HCNAl reaction product and a second HCN. Pick-up cell pressure dependence measurements indicate that this band corresponds to 2 HCN's and MP2 calculations for the drawn structure are in qualitative agreement with the molecular constants derived from the simulations of the spectra. See Table 7.

$B = 0.023$ cm^{-1}, which is a factor of 2.64 smaller than that predicted from our 1D potentials including SOC, namely $B_0 = 0.0608$ cm^{-1}. This value for the reduction of B lends supporting evidence to that used for gallium ($B_{red} = 2.98$), where there is some discrepancy between the experimentally observed and predicted spectra. Interestingly, there is no Q-branch feature observed for HCN−In, in agreement with that predicted by the simulations, hinting that the HCN−Ga spectrum is indeed perturbed by the helium droplet. On the basis of the simple pattern of rational transitions, we can say that the parity doubling constant $p \sim 2B$.

HCN−Al → HCNAl. Careful searches in the HCN free stretching region did not reveal evidence of a nitrogen-bound HCN−Al complex in contrast to our gallium and indium results. Instead, several weaker features are observed, which optimized at higher HCN pressures and are thus related to higher-order $(HCN)_{(n>1)}$−Al complexes. One possibility for the lack of formation of a HCN−Al complex is that the reaction is barrierless, or that the helium cannot quench the energy fast enough to trap the reactants behind the entrance channel barrier. In contrast to our calculations on HCN−Ga, geometry optimizations for HCN−Al at the RCCSD(T)/aug-cc-pVTZ level, where linearity is enforced, yield one imaginary frequency indicating this geometry is a first-order transition state. Fully relaxed calculations starting from linear HCN−Al converged to HCNAl, suggesting that the reaction has a very small barrier if at all.

Unfortunately, the tuning range of the FCL used in this work prevents us from searching directly for the reacted complexes, as predicted by the harmonic frequency calculations summarized in Table 2. As noted above, several weaker peaks are observed in the pendular survey scans, which can be attributed to aluminum bearing complexes with more than one HCN. We propose that these peaks are the result of reaction of HCN+Al, to form one of the four different products, and then a second HCN is picked up by the droplet to form a weakly bound complex, which maintains its high-frequency CH stretch. That this may be possible is due to the unique growth process in helium. Due to the multitude of possible reaction products and the multidimensional potential associated with the second HCN, there are many possible structures. For the pendular peak at 3266 cm^{-1} we were able to record field-free and Stark spectra, which are shown in Figure 11A,C, respectively. The Stark spectrum was recorded in the presence of a 5.103 kV cm^{-1} electric field. Molecular parameters derived from the fits to the spectra are given in Table 7. On the basis of the fact that the

TABLE 7: Summary of the Experimental and UMP2 Molecular Properties of the Complex between HCNAl and a Second HCN That is Weakly Bound to the Al in a Hydrogen-Bonded Arrangement[a]

constant	UMP2/aug-cc-pVDZ	experiment
ν_0 (cm^{-1})	3260.56	3266.68
B (cm^{-1})	0.0223	0.0093
μ (D)	3.54	3.5(3)

[a] The calculated band origin has been scaled to the HCN monomer band origin in helium. The experimental rotational constant is reduced by a factor of 2.4 compared to the calculations, which is necessary to account for the effects of the helium, providing additional support for our assignment.

spectrum resembles a linear rotor, and that the band origin is in the hydrogen-bonded frequency region of HCN, we searched via *ab initio* calculations for possible products to compare with the experimental results. A reaction product that shows excellent agreement with the experimental data is shown in Figure 11, and its calculated properties are summarized in Table 7. Although the complex is not exactly linear, the resulting *A* rotational constant would be too large to allow significant population in the excited *K* states at the temperature of the droplets, and thus the resulting $K = 0 \leftarrow 0$ band would be indistinguishable from that of a linear rotor. The agreement with theory is excellent lending strong support to this assignment. Several other small peaks are observed and could be related to more structures of this type. Apparently, the barrier in this system is low enough that the reaction takes place for aluminum, and no HCN−Al is formed. On the basis of the observation of the HCN−Ga and HCN−In complexes, we infer that the barriers to these reactions are larger allowing stabilization of at least some nitrogen-bound prereactive complexes. Repeating these experiments using an appropriate laser source that can probe the reaction products directly will allow one to determine if any gallium or indium reaction products are formed upon the initial condensation within the droplet.

Discussion

We begin this discussion by examining several observations for the hydrogen-bound M−HCN complexes. When one compares the vibrational frequencies of the fundamentals in each of the Al, Ga, and In−HCN complexes (3192, 3200, and 3219 cm^{-1}), we see that the band origin is shifting nonlinearly to the blue as one goes down the periodic table, a trend that is opposite

to that observed in our earlier halogen work (X–HCN[45] and X–HF[63]). A large red shift in frequency for a hydrogen-bound HCN complex can be shown to be a result of an interaction that weakens the CH bond, which for this atom–molecule system results mostly from a dipole–quadrupole interaction of the form[64]

$$V_Q \propto \frac{\langle r_a^2 \rangle \mu_{HCN}}{R^4} \qquad (1)$$

$\langle r_a^2 \rangle$ is the mean square radius of the incomplete atomic shell, which is related to the quadrupole moment of the open shell atom (Θ_a) by $\Theta_a = {}^2/_5 e \langle r_a^2 \rangle$. *Ab initio* calculations on the X–HCN and X–HF complexes reveal that the complexes have increasingly larger binding energies as one goes down the periodic table, which we attribute to the increasing halogen atom quadrupole moments. Note that the distance between the halogen atom and the HCN center of mass also increases as one goes down the periodic table however the increase in Θ_a overwhelms this effect. A similar argument might be applied to the metal atom complexes and predict that the heavier metal atoms would also have larger binding energies, and a correspondingly larger red shift of the HCN vibrational frequency. These trends are partly predicted in our nonrelativistic *ab initio* calculations for gallium and aluminum; namely, Ga–HCN is predicted to be further red-shifted from HCN monomer than Al–HCN. For In–HCN, however, it appears that the increased van der Waals radius becomes important, making the interaction somewhat weaker. Such a trend in vibrational band origins is not observed experimentally. Gallium atoms do have a larger quadrupole moment than aluminum atoms, however, the dominant interaction here is the SOC, making the overall interaction weaker as we go down the periodic table (see Table 5 for details), producing a smaller effect on the H–CN vibrational frequency as the SOC increases. For the halogen complexes (X–HCN) this interaction is not as important because the ground-state configuration is $^2\Pi_{3/2}$, which does not interact via a first-order process with the $^2\Sigma_{1/2}$ state. For M–HCN, the ground state is predicted to be $^2\Sigma_{1/2}$, which is perturbed by the $^2\Pi_{1/2}$ state by off-diagonal SOC.

To estimate the contribution to the frequency shift resulting from an increase in the binding energy of the complex we compare the bound states from the 1D potential energy surfaces with the HCN restricted in a $v = 0$ or $v = 1$ like geometry, as we did for the nitrogen-bound complexes. One can see the spin–orbit corrected binding energies of the complexes decrease in the order of Al > Ga > In, in good agreement with the ordering predicted on the basis of the frequency shifts. Based solely on the differences in binding energies in the ground and excited vibrational states, the calculations predict red shifts of 45.07 (21.13), 46.42 (37.89), and 44.01 (43.86) cm^{-1} for the (spin–orbit corrected) $^2\Sigma_{1/2}$ potential energy surfaces of In–HCN, Ga–HCN, and Al–HCN, respectively. Clearly these frequency shifts are much smaller than observed experimentally illustrating that the coupling of R and r_{CH} is not negligible, as one might have expected for a hydrogen-bound isomer. Frequency shifts based on the non-spin–orbit corrected potentials agree with the relative ordering predicted by the harmonic frequency calculations, namely Ga–HCN > Al–HCN > In–HCN, but disagree with our experimental results. The relative ordering predicted from our spin–orbit corrected potentials, namely Al–HCN > Ga–HCN > In–HCN, is in agreement with our results, illustrating that SOC cannot be neglected. Despite the large difference between our 1D calculations and experimental results for the

absolute magnitude of the frequency shift, when SOC is incorporated the relative spacing of the different metal atom complexes is reproduced quite well: $\nu_{Ga-HCN} - \nu_{Al-HCN} = 6.12$ cm^{-1} and $\nu_{In-HCN} - \nu_{Ga-HCN} = 16.76$ cm^{-1}, compared to 7.93 and 19.1 cm^{-1} observed experimentally.

To interpret all of the observed features in our spectra, we have assigned three peaks to combination bands on the basis of their agreement with theoretical calculations. What is slightly unusual about this assignment is that the combination band intensities are comparable to the fundamentals, whereas typically combination bands are much weaker. For these open shell complexes, however, an additional source of mechanical anharmonicity may come from state mixing induced by SOC, possibly resulting in the combination band borrowing intensity from the fundamental CH stretching vibration. Clearly a theoretical prediction of the intensities for these combination bands would be helpful to further our understanding of the couplings present in these multidimensional potential energy surfaces.

Interestingly, only the intermolecular stretch combination bands have been observed for the M–HCN complexes, whereas the corresponding intermolecular bending combinations bands are missing. For Al–HCN this is due to the fact that our survey scans did not cover the appropriate frequency region ($\nu_{bend} = 192$ cm^{-1} at the RCCSD(T)/aug-cc-pVTZ level); however the bend combinations for both Ga–HCN ($\nu_{bend} = 76.7$ cm^{-1}) and In–HCN should be located in this frequency region. Because the survey scans in Figure 9 were recorded under pendular conditions, vibrational modes with transition moments parallel to the permanent dipole moment show an enhancement in strength due to an orientational effect by the field. If the vibrational transition moment angle for the bend combination band is greater than the magic angle, 54.7°, these bands will weaken with the applied field, possibly preventing their observation. Clearly revisiting these experiments using perpendicular polarization would be helpful in determining if these combination bands can be observed.

Summary

In this study helium nanodroplets have been applied to the stabilization of the highly reactive entrance channel complexes between aluminum, gallium, and indium atoms and a single HCN molecule. These complexes may be particularly hard to stabilize using other methods due to the fact that the barriers to reaction are so small, and are predicted to lie lower in energy than separated M + HCN. The small barriers to reaction give rise to an ideal scenario to probe the effects of long-range forces and tunneling on reaction dynamics at ultracold temperatures. Theoretical calculations predict two linear van der Waals complexes for gallium and indium atoms with HCN whereas for aluminum, the nitrogen-bound isomer was found to fall into a reaction product well (HCNAl). Experimentally, the nitrogen-bound HCN–Ga and HCN–In complexes as well as the hydrogen-bound Al–HCN, Ga–HCN, and In–HCN complexes have been observed in good agreement with theory. The lack of the corresponding HCN–Al isomer is attributed to reaction, even at 0.37 K. The rotationally resolved spectra of HCN–Ga and HCN–In do not fit well to a standard Hund's case (a) $^2\Pi_{1/2}$ model, and we attribute this to an off-diagonal spin–orbit interaction with the $^2\Sigma_{1/2}$ state, which gives rise to large parity splittings. In the indium spectrum, the SOC is so large that the spectrum is best described using a Hund's case (c) formalism. Using a one-dimensional treatment, we can qualitatively reproduce the parity splitting, which brings the agreement of the

Al−, Ga−, In−HCN Entrance Channel Complexes

J. Phys. Chem. A, Vol. 111, No. 49, 2007 **12315**

observed rotational constant into good agreement with theoretical calculations. The HCN−Ga spectrum has a large Q branch feature at the band origin that is not reproduced by the simulations and we attribute this to a helium droplet interaction.

Two vibrational modes of the Al−HCN, Ga−HCN, and In−HCN complexes are observed and assigned to the fundamental CH stretching vibration of the linear hydrogen-bound isomer and a combination band of CH plus intermolecular stretches. Bound states on spin−orbit corrected 1D (intermolecular stretch) potential energy surfaces are presented and are in excellent agreement with the experimental frequencies for the van der Waals stretch.

Due to limitations of our laser source, the reaction products could not be directly probed. Rotationally resolved spectra for a band at 3266 cm^{-1} were obtained, which we can definitively assign to a complex between an Al atom with two HCN molecules. On the basis of the agreement with theory, we assign this peak to a weakly bound complex of HCNAl, with a second HCN. The unique growth processes in helium allow for the stabilization of such exotic cluster systems.

Building on the characterization of these reactive potential energy surfaces, we have experimentally probed the reaction, isomerization, and vibrational relaxation dynamics of these entrance channel complexes, which will be the subject of a future publication.

References and Notes

(1) Skouteris, D.; Manolopoulos, D. E.; Bian, W.; Werner, H. J.; Lai, L. H.; Liu, K. *Science* **1999**, *286*, 1713−1716.

(2) Balakrishnan, N.; Dalgarno, A. *Chem. Phys. Lett.* **2002**, *341*, 652−656.

(3) Balakrishnan, N. *J. Chem. Phys.* **2004**, 121 (12), 5563−5566.

(4) Weck, P. F.; Balakrishnan, N. *J. Chem. Phys.* **2005**, *123*, 144308.

(5) Weck, P. F.; Balakrishnan, N. *Int. Rev. Phys. Chem.* **2006**, *25*, 283.

(6) Towsend, D.; Lahankar, S. A.; Lee, S. K.; Chambreau, S. D.; Suits, A. G.; Zhang, X.; Rheinecker, J.; Harding, L. B.; Bowman, J. M. *Science* **2005**, *306*, 1158.

(7) Hutson, J. M. *Annu. Rev. Phys. Chem.* **1990**, *41*, 123−154.

(8) Tsiouris, M.; Wheeler, M. D.; Lester, M. I. *J. Chem. Phys.* **2001**, *114* (1), 187−197.

(9) Lester, M. I.; Pond, B. V.; Marshall, M. D.; Anderson, D. T.; Harding, L. B.; Wagner, A. F. *Faraday Discuss.* **2001**, *118*, 373−385.

(10) Wheeler, M. D.; Anderson, D. T.; Lester, M. I. *Int. Rev. Phys. Chem.* **2000**, *19* (4), 501−529.

(11) Chen, Y. L.; Heaven, M. C. *J. Chem. Phys.* **1998**, *109* (13), 5171−5174.

(12) Fawzy, W. M.; Kerenskaya, G.; Heaven, M. C. *J. Chem. Phys.* **2005**, *122*, 144318.

(13) Vissers, G. W. M.; McCoy, A. B. *J. Phys. Chem. A* **2006**, *110*, 5978−5981.

(14) Choi, M. Y.; Douberly, G. E.; Falconer, T. M.; Lewis, W. K.; Lindsay, C. M.; Merritt, J. M.; Stiles, P. L.; Miller, R. E. *Int. Rev. Phys. Chem.* **2006**, *25* (1), 15−75.

(15) Küpper, J.; Merritt, J. M. *Int. Rev. Phys. Chem.* **2007**, 26 (2), 249−287.

(16) Jones, P. M.; Kasai, P. H. *J. Phys. Chem.* **1988**, *92*, 1060−1061.

(17) Lanzisera, D. V.; Andrews, L. *J. Phys. Chem. A* **1997**, *101*, 9660−9665.

(18) Burkholder, T. R.; Andrews, L. *Inorg. Chem.* **1993**, *32* (11), 2491−2496.

(19) Jursic, B. S. *Chem. Phys.* **1998**, *237*, 51−58.

(20) Sakai, S. *J. Phys. Chem.* **1992**, *96*, 8369−8373.

(21) McKee, M. L. *J. Am. Chem. Soc.* **1993**, *115* (21), 9608−9613.

(22) Fängström, T.; Lunell, S.; Kasai, P. H.; Eriksson, L. A. *J. Phys. Chem. A* **1998**, *102*, 1005−1017.

(23) Swihart, M. T.; Catoire, L. *J. Phys. Chem. A* **2001**, *105*, 264−273.

(24) Xie, Y. M.; Yates, B. F.; Schaefer, H. F. *J. Am. Chem. Soc.* **1990**, *112* (2), 517−523.

(25) Lanzisera, D. V.; Andrews, L. *J. Phys. Chem. A* **1997**, *101*, 7134−7140.

(26) Nauta, K.; Miller, R. E. *J. Chem. Phys.* **1999**, *111*, 3426−3433.

(27) Knuth, E. L.; Schilling, B.; Toennies, J. P. *On Scaling Parameters for Predicting Cluster Sizes in Free Jets*; Oxford University Press: Oxford, U.K., 1995; Vol. 19.

(28) Lewerenz, M.; Schilling, B.; Toennies, J. P. *J. Chem. Phys.* **1995**, *102*, 8191−8207.

(29) Claas, P.; Mende, S. O.; Stienkemeier, F. *Rev. Sci. Instrum.* **2003**, *74* (9), 4071−4076.

(30) Reho, J. H.; Merker, U.; Radcliff, M. R.; Lehmann, K. K.; Scoles, G. *J. Phys. Chem. A* **2000**, *104*, 3620−3626.

(31) Hui, Q.; Perssen, J. L.; Beijersbergen, J. H. M.; Takami, M. *Z. Phys. B* **1995**, *98*, 353.

(32) Kasper, J. V. V.; Pollock, C. R.; Curl, R. F., Jr.; Tittel, F. K. *Appl. Opt.* **1982**, *21*, 236−247.

(33) Huang, Z. S.; Jucks, K. W.; Miller, R. E. *J. Chem. Phys.* **1986**, *85*, 3338−3341.

(34) Brink, D. M.; Stringari, S. *Z. Phys. D* **1990**, *15*, 257−263.

(35) Stiles, P. L.; Nauta, K.; Miller, R. E. *Phys. Rev. Lett.* **2003**, *90* (13), 135301.

(36) Moore, D. T.; Oudejans, L.; Miller, R. E. *J. Chem. Phys.* **1999**, *110*, 197−208.

(37) Douberly, G. E.; Miller, R. E. *J. Phys. Chem. B* **2003**, *107* (19), 4500−4507.

(38) Ochterski, J. W.; Petersson, G. A.; Montgomery, J. A., Jr. *J. Chem. Phys.* **1996**, *104* (7), 2598−2619.

(39) Curtiss, L. A.; Raghavachari, K.; Trucks, G. W.; Pople, J. A. *J. Chem. Phys.* **1991**, *94* (11), 7221.

(40) Frisch, M. J.; Trucks, G. W.; Schlegel, H. B.; Scuseria, G. E.; Robb, M. A.; Cheeseman, J. R.; Montgomery, J. A., Jr.; Vreven, T.; Kudin, K. N.; Burant, J. C.; Millam, J. M.; Iyengar, S. S.; Tomasi, J.; Barone, V.; Mennucci, B.; Cossi, M.; Scalmani, G.; Rega, N.; Petersson, G. A.; Nakatsuji, H.; Hada, M.; Ehara, M.; Toyota, K.; Fukuda, R.; Hasegawa, J.; Ishida, M.; Nakajima, T.; Honda, Y.; Kitao, O.; Nakai, H.; Klene, M.; Li, X.; Knox, J. E.; Hratchian, H. P.; Cross, J. B.; Adamo, C.; Jaramillo, J.; Gomperts, R.; Stratmann, R. E.; Yazyev, O.; Austin, A. J.; Cammi, R.; Pomelli, C.; Ochterski, J. W.; Ayala, P. Y.; Morokuma, K.; Voth, G. A.; Salvador, P.; Dannenberg, J. J.; Zakrzewski, V. G.; Dapprich, S.; Daniels, A. D.; Strain, M. C.; Farkas, O.; Malick, D. K.; Rabuck, A. D.; Raghavachari, K.; Foresman, J. B.; Ortiz, J. V.; Cui, Q.; Baboul, A. G.; Clifford, S.; Cioslowski, J.; Stefanov, B. B.; Liu, G.; Liashenko, A.; Piskorz, P.; Komaromi, I.; Martin, R. L.; Fox, D. J.; Keith, T.; Al-Laham, M. A.; Peng, C. Y.; Nanayakkara, A.; Challacombe, M.; Gill, P. M. W.; Johnson, B.; Chen, W.; Wong, M. W.; Gonzalez, C.; Pople, J. A. *Gaussian 03*, revision A.1; Gaussian: Wallingford, CT, 2003.

(41) Lee, T. J.; Taylor, P. R. *Int. J. Quantum Chem. Symp.* **1989**, *23*, 199.

(42) Werner, H. J.; Knowles, P. J.; Almlof, J.; Amos, R. D.; Berning, A.; Deegan, M. J. O.; Eckert, F.; Elbert, S. T.; Hampel, C.; Lindh, R.; Meyer, W.; Nicklass, A.; Peterson, K.; Pitzer, R.; Stone, A. J.; Taylor, P. R.; Mura, M. E.; Pulay, P.; Scheutz, M.; Stoll, H.; Thorsteinsson, T.; Cooper, D. L. *MOLPRO, a package of ab initio programs*, number 2002.1, 2002.

(43) Boys, S. F.; Bernardi, F. *Mol. Phys.* **1970**, *19* (4), 553−566.

(44) Fishchuk, A. V.; Merritt, J. M.; Groenenboom, G. C.; van der Avoird, A. *J. Phys. Chem. A*, in press.

(45) Merritt, J. M.; Küpper, J.; Miller, R. E. *Phys. Chem. Chem. Phys.* **2007**, *9*, 401−416.

(46) Cramer, C. J. *Essentials of computational chemistry: theories and models*; J. Wiley and Sons: New York, 2002.

(47) Peterson, K. A.; Figgen, D.; Goll, E.; Stoll, H.; Dolg, M. *J. Chem. Phys.* **2003**, *119* (21), 11113−11123.

(48) Zeimen, W. B.; Klos, J.; Groenenboom, G. C.; van der Avoird, A. *J. Phys. Chem. A* **2003**, *107*, 5110−5121.

(49) Meuwly, M.; Hutson, J. M. *Phys. Chem. Chem. Phys.* **2000**, *2* (4), 441−446.

(50) Klos, J.; Chalasinski, G.; Werner, H.; Szczesniak, M. M. *J. Chem. Phys.* **2003**, *115* (7), 3085−3098.

(51) Lefebvre-Brion, H.; Field, R. W. *Perturbations in the Spectra of Diatomic Molecules*; Academic Press: Orlando, FL, 1986.

(52) LeRoy, R. J. Level 7.7: A computer program for solving the radial schrödinger equation for bound and quasibound levels University of Waterloo Chemical Physics Research Report CP-661; see the "computer programs" link at http://leroy.uwaterloo.ca, 2005.

(53) Nauta, K.; Miller, R. E. *Science* **1999**, *283*, 1895−1897.

(54) Hartmann, M.; Miller, R. E.; Toennies, J. P.; Vilesov, A. F. *Phys. Rev. Lett.* **1995**, *75*, 1566−1569.

(55) Nauta, K.; Miller, R. E. *J. Chem. Phys.* **2001**, *115* (22), 10254−10260.

(56) Schmied, R.; Carcabal, P.; Dokter, A. M.; Lonij, V. P. A.; Lehmann, K. K.; Scoles, G. *J. Chem. Phys.* **2004**, *121*, 2701−2710.

Merritt et al.

(57) Merritt, J. M. Ph.D. Dissertation, University of North Carolina at Chapel Hill, 2006.

(58) Draeger, E. W.; Ceperley, D. M. *Phys. Rev. Lett.* **2003**, *90* (6), 065301.

(59) Nauta, K.; Moore, D. T.; Miller, R. E. *Faraday Discuss.* **1999**, *113*, 261−278.

(60) Paesani, F.; Whaley, K. B.; Douberly, G. E.; Miller, R. E. *J. Phys. Chem. A*, in press.

(61) von Haeften, K.; Metzelthin, A.; Rudolph, S.; Staemmler,V.; Havenith, M. *Phys. Rev. Lett.* **2005**, *95* (21), 215301.

(62) Douberly, G. E.; Merritt, J. M.; Miller, R. E. *Phys. Chem. Chem. Phys.* **2005**, *7* (3), 463−468.

(63) Merritt, J. M.; Küpper, J.; Miller, R. E. *Phys. Chem. Chem. Phys.* **2005**, *7* (1), 67−78.

(64) Meuwly, M.; Hutson, J. M. *J. Chem. Phys.* **2003**, *119*, 8873−8881.